Mai, Sebastian; Wessel, Janine; Dimitrova, Anna; Stich, Michael; Ivanov, Svetlozar; Krischok, Stefan; Bund, Andreas:

Nanoscale morphological changes at lithium interface, triggered by the electrolyte composition and electrochemical cycling

Research Article

Nanoscale Morphological Changes at Lithium Interface, Triggered by the Electrolyte Composition and Electrochemical Cycling

Sebastian Mai,[1] Janine Wessel,[1] Anna Dimitrova,[2] Michael Stich,[1] Svetlozar Ivanov [ID],[1] Stefan Krischok,[2] and Andreas Bund[1]

[1]*Electrochemistry and Electroplating Group, Technische Universität Ilmenau, Ilmenau 98693, Germany*
[2]*Institute of Physics and Institute of Micro- and Nanotechnologies MacroNano, Technische Universität Ilmenau,*
 PF 100565, 98684 Ilmenau, Germany

Correspondence should be addressed to Svetlozar Ivanov; svetlozar-dimitrov.ivanov@tu-ilmenau.de

Understanding the electrochemical and morphological properties of the Li-electrolyte interface plays a central role in the implementation of metallic Li in safe and efficient electrochemical energy storage. The current study explores the influence of soluble polysulfides (PS) and lithium nitrate ($LiNO_3$) on the characteristics of the solid electrolyte interphase (SEI) layer, formed spontaneously on the Li surface, prior to electrochemical cycling. Special attention is paid to the evolution of the electrochemical impedance and nanoscale morphology of the interface, influenced by the contact time and electrolyte composition. The basic tools applied in this investigation are electrochemical impedance spectroscopy (EIS), atomic force microscopy (AFM) performed at the nanoscale, and X-ray photoelectron spectroscopy (XPS). The individual addition of polysulfides and $LiNO_3$ increases the interface resistance, while the simultaneous application of these components is beneficial, reducing the SEI resistive behavior. The electrochemical cycling of Li in nonmodified 1,2-dimethoxy ethane (DME) and tetraethylene glycol dimethyl ether (TEGDME) based electrolytes leads to slight morphological changes, compared to the pristine Li pattern. In contrast, we found that in the presence of PS and $LiNO_3$, the interface displays a rough and inhomogeneous morphology.

1. Introduction

Metallic lithium is, in principle, the best anode material for any Li-ion battery. It delivers a theoretical capacity of $3860 \, mAhg^{-1}$ at the lowest possible potential ($-3.04 \, V$ vs. SHE). However, most organic electrolytes are chemically unstable against lithium. Furthermore, dendrite formation and low lithium cycling efficiency create safety and operational risks. It is believed that the latter problems result from the instability of the passivation layer (solid electrolyte interphase, SEI) formed on the metallic anode [1, 2]. During electrochemical cycling, the SEI cannot accommodate the shape and volume changes at the metal interface, and thus a nonuniform lithium deposition and dissolution takes place.

Additionally, the instability of the SEI causes a frequent exposure of bare Li metal to the electrolyte, forming new passivation layers and promoting further electrolyte depletion [3].

When Li metal is used as an anode, it is no longer reasonable to implement organic carbonates as solvents. Most of them continuously decompose on the Li surface and do not form a stable passivation layer [4, 5]. Instead, it is practical to apply ether-based electrolytes, which are commonly implemented in lithium-sulfur batteries due to the low lithiation potential of sulfur. Furthermore, they offer the possibility to stabilize the Li-electrolyte interface. The most frequently used ether compound in Li-S systems is 1,3-dioxolan (DOL), a main component of binary mixtures with

1,2-dimethoxy ethane (DOL/DME) or tetraethylene glycol dimethyl ether (DOL/TEGDME). TEGDME-based electrolytes visibly enhance the sulfur utilization, leading to higher capacity of the lithium-sulfur battery [6].

The growth of Li-on-Li depends on the current density and electrolyte composition [1]. Thereby, its morphology changes from mossy (growth from the root of the Li filaments) to dendritic (in a classical fast top-growth way). None of those growth mechanisms is ideal for a lithium metal anode, and realizing a uniform plating is still a big challenge. In lithium-sulfur cells, the mossy-like growth is typically not a concern, even at high current densities [2]. This effect is attributed to the synergistic influence of (1) the dissolved PS, (2) the commonly used sulfonamide lithium salts (i.e., lithium bis(trifluoromethanesulfonyl) imide, LiTFSI), and (3) the addition of lithium nitrate [2, 7].

The electrochemical behavior of TFSI has become a popular research object since the emergence of ionic liquids in chemistry applications [8–12]. Aurbach et al. [8] showed that while being stable at the battery operating voltage, TFSI decomposes on lithium metal into various species, where the main decomposition component that stabilizes the Li-electrolyte interface is lithium sulfate. However, it was further suggested that the decomposition of LiTFSI does not result in a high enough sulfate concentration to passivate the metal surface efficiently. For that reason, lithium nitrate is added to the electrolyte, which supports the oxidation of the PS species to lithium sulfates and additionally yields substoichiometric lithium nitrates (Li_xNO_y, $2 > x > 1$, $3 > y > 1$). It turned out that the structure built from the substoichiometric lithium nitrates and sulfates is a good Li-ion conductor, which is essential for the SEI performance [8].

Due to the high reactivity of metallic Li, its interaction with the electrolyte starts spontaneously, immediately after the contact with electrolyte. Li anode self-passivation is in any case the first chemical phenomenon that occurs when a battery with metallic Li is assembled. The process is essential for the battery performance, and therefore, it is highly important to better understand its mechanism. The electrical and morphological properties of this initial SEI layer can significantly vary depending on the electrolyte constituents and time. The self-passivation of Li metal in DOL-based electrolytes is generally regarded as stabilizing within a few hours [6, 13, 14]. However, the exact formation time of the stable SEI and the interfacial resistance of the resulting layer are important for the battery performance and depend on the applied additive (i.e., $LiNO_3$, PS, and ionic liquid). While the self-passivating phenomena on the Li surface have been investigated in a few recent studies by impedance spectroscopy, the information on the initial chemical composition and SEI microstructure, further influenced by electrochemical cycling, is incomplete. The surface film deposition on Li has been analyzed in LiTFSI, DOL : DME-based electrolytes by SPM and XPS, where the focus is set on the influence of $LiNO_3$, without exploring the interface properties after cycling [15]. Additionally, the surface morphology and composition of Li interface are studied only in LiTFSI, DOL : TEGDME-based electrolyte [16]. However,

the effect of $LiNO_3$ and PS as additives is highly important to completely understand the Li interfacial phenomena in this electrolyte type. Since it increases the ionic conductivity and improves the sulfur utilization, TEGDME has a valuable input as a solvent component in the electrolytes for Li-S batteries [17].

In the current contribution, we intend to complete the entire overview on Li surface-passivating phenomena in LiTFSI, DOL : TEGDME, involving the influence of additives. We study the time evolution of the electrical properties of the SEI, spontaneously formed on Li metal in the presence of PS, $LiNO_3$, and PS + $LiNO_3$ and perform a direct AFM observation of the SEI topology at nanoscale. A correlation between the interfacial resistance and chemical composition provided by XPS has been performed. The differences in electrical, morphological, and chemical properties of the Li interface before (after self-passivation) and after electrochemical cycling are discussed. According to our literature survey, there is no earlier scientific contribution on the surface topology of the Li interface, influenced by the existence of additives in TEGDME-based electrolytes.

2. Materials and Methods

The electrolyte solvents (analytical grade DOL, DME, and TEGDME), LiTFSI, elemental sulfur, and Li metal foil (99.9%) with a thickness of 0.75 mm were purchased from Alfa Aesar. The solvents and electrolytes necessary for electrochemical experiments were dried with a molecular sieve (pore diameter 0.3 nm) until a value lower than 15 ppm H_2O was reached. The moisture in the electrolytes was measured by Karl-Fischer titration (831 KF Coulometer, Metrohm).

The electrolyte was composed of 1 M LiTFSI dissolved in DOL : TEGDME (7 : 3 w/w). This composition was used as a reference electrolyte, which was further modified with $LiNO_3$, PS, and a combination of both additives. The concentration of $LiNO_3$ was 0.2 M for the additive containing electrolytes, and the concentration of PS was 1% (w/w), calculated with respect to the elemental sulfur used for the PS preparation. Stoichiometric quantities of elemental sulfur and lithium metal, 3 : 1, respectively, were used for the preparation of PS solution in DOL : TEGDME (7 : 3 w/w).

Li chips with the diameter 11 mm and area 0.98 cm^2 were used for the self-passivation processes and for the electrochemical cycling. The substrates were dipped in equal volumes (5 ml) of each electrolyte (1 M LiTFSI DOL : TEGDME; 1 M LiTFSI DOL : TEGDME + 0.2 M $LiNO_3$; 1 M LiTFSI DOL : TEGDME + PS; and 1 M LiTFSI DOL : TEGDME + 0.2 M $LiNO_3$ + PS) for 1 h, 5 h, and 10 h contact time in closed vials under Ar atmosphere. After the treatment in the electrolytes, the samples were washed with DOL, dried under vacuum, and further analyzed by XPS and AFM. The same electrolytes were used for monitoring the self-passivation phenomena by impedance spectroscopy and constant current cycling in symmetric Li-Li cells.

Symmetric, Swagelok-type cells, used for EIS and galvanostatic cycling, were filled with electrolyte and assembled each with two identical Li metal anodes with a Celgard separator in between. The EIS spectra were recorded with a BioLogic VMP3 potentiostat in the frequency range of 5 mHz–400 kHz with 5 points per decade and a 10 mV excitation amplitude. For parameter analysis, only the high-to-medium frequency range (100 Hz–400 kHz) is used. The low-frequency domain, which is usually represented by a Warburg-impedance part, is neglected due to the highly unreliable fit with conventional methods. Series of samples for AFM analysis were prepared by symmetric Li vs. Li galvanostatic cycling at $j = 0.5$ mA·cm^{-2} for 6 cycles.

In a separate experimental series, Li was 20 times galvanostatically cycled at C/2 against cathode coating, containing 10% carbon black (Timical SUPER C65), 6% guargum (Asgra UG), and 84% nanocarbon-sulfur composite (supplied by cooperation partner, 45% S).

After 10 h spontaneous SEI formation and washing and drying in the argon-filled glove box, the samples for XPS were transferred in an inert gas transport box to the load lock vacuum system followed by direct evacuation to avoid exposure to air and ambient conditions. XPS analysis was carried out with a Specs SAGE spectrometer (base pressure $<1 \times 10^{-8}$ mbar) equipped with a Phoibos 150 electron analyzer using a focused monochromatic AlKα radiation ($h\nu = 1486.7$ eV). During the experiments, the pressure in the analysis chamber was $\sim 5 \times 10^{-8}$ mbar. Core level spectra were recorded at a constant analyzer pass energy of 13 eV allowing a total energy resolution of 0.6 eV (Ag3d$^{5/2}$ of the Ag reference sample), and no charge neutralization was used. For binding energy calibration, the energy scale was corrected by aligning the C1s signal at 285.0 eV [18]. The core-level spectra were analyzed by subtracting a Shirley-type background [19], and peak areas were calculated by a weighed least-square fitting of model curves (70% Gaussian, 30% Lorentzian) to the experimental data using the software package CASA XPS (Version 23.16 Dev52, Casa Software Ltd.). For quantification, the atomic percentage (at. %) was calculated based on photoionization cross sections [20]. XPS sputter profiling was performed using a differentially pumped IQE 12/38 ion source operated with Argon (source pressure 2.2×10^{-3} mBar, Ar$^+$ ion energy 3 keV, 10 mA emission current, 6 mA ion current) and laterally scanning the Ar$^+$ ions across the sample surface (scan area 10×10 mm^2). Under these conditions, the SEI layer can be etched at a rate of ~ 0.2–0.3 nm·min^{-1}.

The AFM measurements were conducted with a Bruker Dimension Icon AFM inside an argon-filled glove box from MBRAUN with H$_2$O and O$_2$ concentrations below 0.1 ppm. The AFM data were obtained in the peak force tapping mode. All displayed AFM images underwent a third-order polynomial flattening procedure using the NanoScope Analysis software by Bruker to remove tilt and curvature. The fast scan direction in all images is horizontal. Complete information regarding the AFM setup can be found in [21].

3. Results and Discussion

3.1. Spontaneous Formation of SEI Layer. A series of impedance measurements in symmetric Li-Li cell arrangement at OCP (less than 2 mV) has been performed in the reference electrolyte 1 M LiTFSI, DOL : TEGDME (7 : 3 vol.). This electrolyte is modified subsequently by LiNO$_3$, PS, and a mixture of both components. The prepared new electrolyte solutions are used for three additional sets of EIS measurements. The spectra are recorded every 30 minutes up to a total duration of 20 hours. For a better visibility, reduced number of impedance curves is shown (Figure 1). The evolution of the Nyquist spectra with time is presented in the Supplementary Materials, SM (Figure S1). The Nyquist plots of the EIS in symmetric cell, shown in Figure 1(a), are fitted by an equivalent circuit consisting of one resistor (R_{cell}) connected in series with a parallel circuit of a constant phase element and a resistor (C_{dl}/R_{ct}), which is also in series with a parallel circuit of a capacitor and a resistor (C_{int}/R_{int}), shown in Figure 1(a). The equivalent circuit is visualized as two overlapping semicircles in the middle frequency domain with an initial offset in the high-frequency domain (Figure 1(a)).

When comparing the time evolution of the impedance, it can be observed that the Li interface undergoes an initial fast buildup of SEI resistance R_{int} in all electrolytes, shown in Figure 1(b). While R_{int} increases visibly over time, approaching saturation, the charge transfer resistance R_{ct} grows only marginally. After individual addition of PS and LiNO$_3$, the interface resistance R_{int} increases significantly (up to 450 Ω·cm^2) compared to the R_{int} in the reference electrolyte, while the charge transfer resistance R_{ct} rises only until 12–16 Ω. When PS and LiNO$_3$ are simultaneously added to the reference electrolyte, R_{int} drops markedly, approaching a value of 175 Ω·cm^2.

The above-described impedance behavior can also be observed in the Bode frequency plots, presented in Figure 2. The phase minimum at 40 kHz, recorded at the first impedance measurement in the reference electrolyte, shifts over time to 20 kHz (Figure S2, SM). This change is accompanied by a widening in the overall phase minimum (initially from 225 kHz to 1 kHz and further extending to 0.1 kHz after 20 h). The observed widening in the Bode phase diagram stems from the frequency separation of two *RC* time constants (one for each parallel circuit) that were initially nearly identical. The latter effect is more pronounced for the measurements performed in the presence of the individual components PS and LiNO$_3$. After separate addition of PS and LiNO$_3$, the phase angle minimums approach 2 kHz and 10 kHz, respectively, indicating a strong increase of the interfacial impedance. The total impedance Bode diagram demonstrates an insignificant change of Z in the frequency range higher than 1 kHz, where the time constant $R_{ct}C_{dl}$ has been detected. The impedance Z increases dramatically for the frequencies below 1 kHz and further keeps its high value until the low-frequency limit. This indicates that the properties of SEI layer, correlated with $R_{int}C_{int}$ time constant, are responsible for the observed Z enhancement.
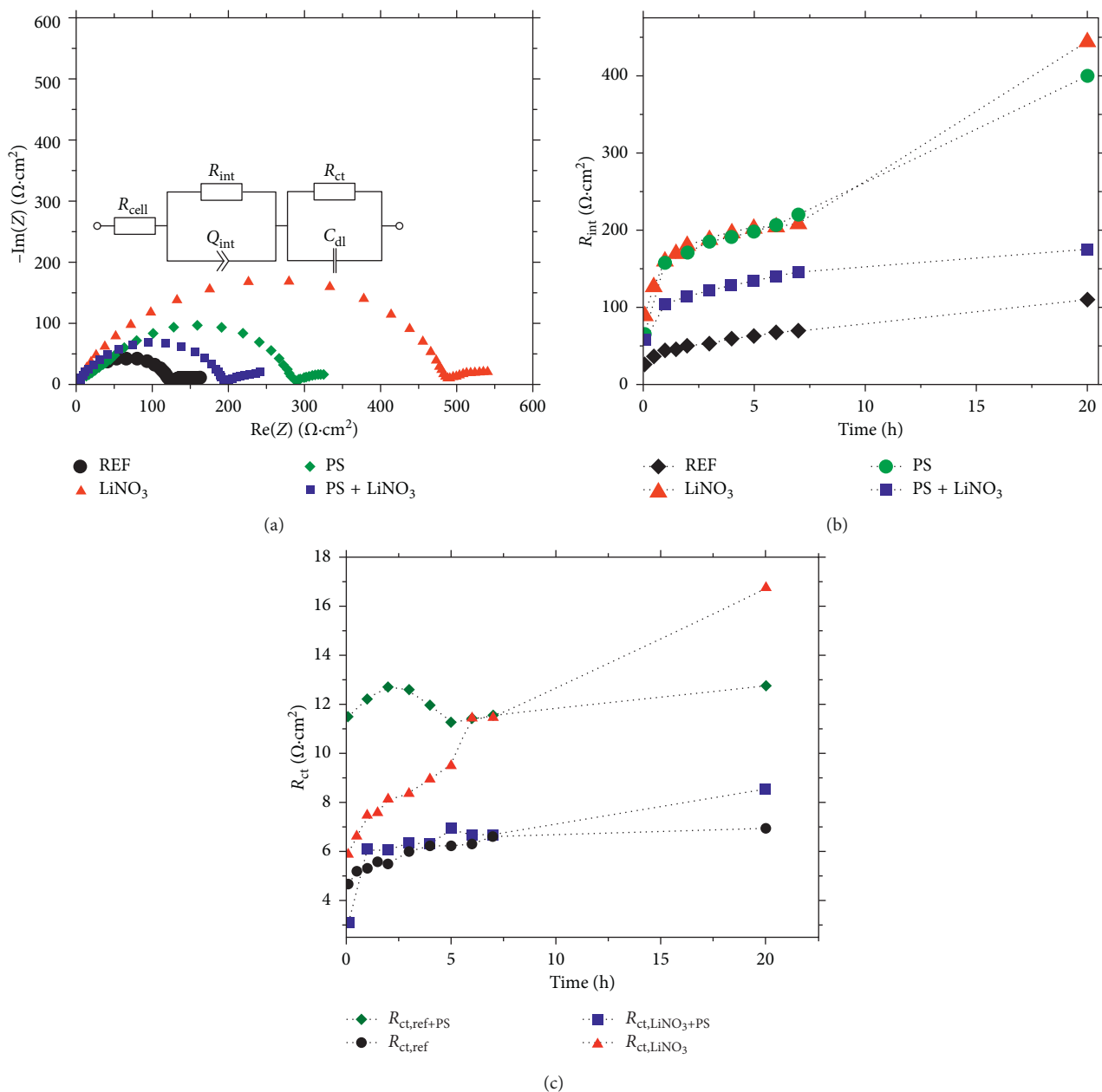
(a)

(b)

(c)

FIGURE 1: Nyquist impedance diagrams for anodes tested in symmetric cells, after 20 h contact time with electrolyte 1 M LiTFSI DOL/ TEGDME (7 : 3) (black); 1 M LiTFSI, 0.2 M LiNO₃, DOL/TEGDME (7 : 3) (red); 1 M LiTFSI, PS DOL/TEGDME (7 : 3) (green); and 1 M LiTFSI, 0.2 M LiNO₃, PS DOL/TEGDME (7 : 3) (blue) (a), interface resistance (R_{int}) (b), and charge transfer resistance (R_{ct}) (c) evaluated for different times.

When comparing the impedance behavior of the Li interface in all electrolytes, it becomes visible that R_{int} in the reference and combined (PS + LiNO₃) electrolytes is much lower. In accordance with the literature, the SEI improving effect of LiNO₃ can only occur when polysulfides are present in the electrolyte [7, 20]. The reason for these drastic changes in the impedance performance should therefore be related to the SEI chemical composition and/ or morphological properties of the deposited layer. Consequently, in the following, we try to reveal the influence of both factors on the electrical/electrochemical properties of

the Li-electrolyte interface by analyzing the Li surface with AFM and XPS.

To enhance the reproducibility of the analysis, the AFM imaging was performed in several experimental sets. However, the strong height inhomogeneity, when working with conventional Li-metal substrates, does not allow exact quantification of the surface roughness, and therefore, the results attained by AFM are used for qualitative comparison. After establishing the contact with the electrolyte, the observed initial pattern changes visibly with time. In both reference media, the surface morphology evolution follows a
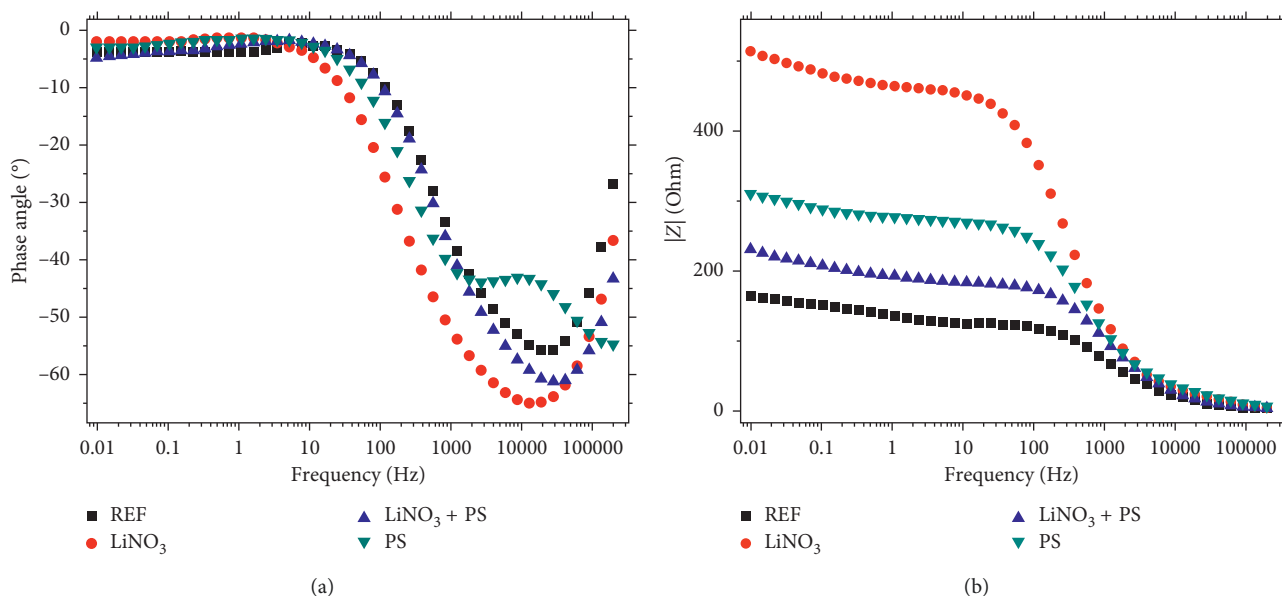
FIGURE 2: Bode phase (a) and total impedance (b) diagrams for anodes tested in symmetric cell, after 20 h contact time with the electrolyte 1 M LiTFSI, DOL/TEGDME (7 : 3) (black); 1 M LiTFSI, 0.2 M LiNO₃, DOL/TEGDME (7 : 3) (red); 1 M LiTFSI, PS DOL/TEGDME (7 : 3) (green); and 1 M LiTFSI, 0.2 M LiNO₃, PS DOL/TEGDME (7 : 3) (blue).

similar trend, resulting in a nanoscale topology and final flattening of the surface (Figure S3). The addition of 0.2 M LiNO$_3$ to the reference electrolyte (1 M LiTFSI, DOL : TEGDME) affects significantly the surface morphology of Li, showing the presence of poorly adhesive SEI layer, formed probably due to the predominance of inorganic sulfate compounds, which are the final product of sulfur oxidation (Figure S4). In general, the addition of polysulfides generates much more irregular surface morphology, probably triggered by the agglomeration of sulfur-containing species (Figures S5 and S6).

The observation by AFM shows that morphological changes at the Li surface result from the spontaneous SEI formation. However, in order to receive information about the SEI chemical composition and related influence of PS and LiNO$_3$ as additives, XPS analysis was performed. C1s, S2p, F1s, and O1s core-level XPS spectra for all four samples are presented in Figure 3.

Figure 4 presents the relative elemental quantities of C, O, F, S, N, and Li on the SEI surface (Figure 4(a)) and after 30 min sputtering, i.e., 6–9 nm in depth (Figure 4(b)). In general, a decrease of carbon and an increase of lithium amounts are observed, when comparing the samples before and after sputtering. Furthermore, while the surface elemental distribution of all four samples is nearly identical (Figure 4(a)), the composition in the bulk differs visibly in respect to O, F, and Li (Figure 4(b)).

In order to discriminate the different chemical species, we performed a detailed XPS analysis of C1s, S2p, O1s, and F1s core-level spectra for all four samples after 30 min sputtering with Ar$^+$. The results of the deconvoluted C1s spectra are presented in Figure 5(a), and the corresponding fitted spectra and their binding energy alignments are shown

in Figure 3(a) and Table 1, respectively. A strong contrast between the carbon species in the SEI formed in the reference electrolyte and in the presence of additives is evident. When LiNO$_3$ is added, the relative amounts of oxidized carbon species (C=O, COR, OCO/COOR, where R is alkyl moiety) and the fluorinated carbon (-CF$_3$) are increased. Since LiTFSI is the sole source of fluorine in the electrolyte, the only possible explanation of this phenomenon can be that LiNO$_3$ favors the decomposition of LiTFSI, in the bulk of the SEI, over the decomposition of TEGDME. This observation is further supported by the parallel decrease of relative C-C signal (Figure 5). The addition of PS in the electrolyte declines the overall percentage of oxidized carbon within the SEI (Figure 5(a)), possibly by being oxidized preferably over carbon. When both LiNO$_3$ and PS are added to the electrolyte, the resulting SEI composition is dissimilar to those gained with one singular component (LiNO$_3$ or PS) used as an additive. It resembles more closely the SEI composition of the reference sample, albeit the addition of LiNO$_3$ leads to reduction in the amount of Li$_2$S (Figure 5(b)) and Li$_2$O (Figure 5(c)). The addition of PS resulted in a slightly higher amount of Li$_2$S$_2$ and S$_x$O$_y$ species but not an increase of total sulfur in the SEI. This suggests the possibility that PS regulates the otherwise boosted decomposition of LiTFSI when LiNO$_3$ is added. The latter can be indicated by the strong gain in CF$_3$ signal (Figure 5(d)) when only LiNO$_3$ is added to the electrolyte. The distribution of sulfur redox states in the SEI's interior can be seen in Figure 5(b). The analysis shows a strong contrast between the electrolyte with individually added LiNO$_3$ and the other samples. While the oxidation states of sulfur are well distributed between −2 in Li$_2$S, −1 in Li$_2$S$_2$, +5 in S$_2$O$_6{}^{2-}$, +4 in SO$_3{}^{2-}$, and +6 in TFSI and SO$_4{}^{2-}$ in samples immersed in the reference,
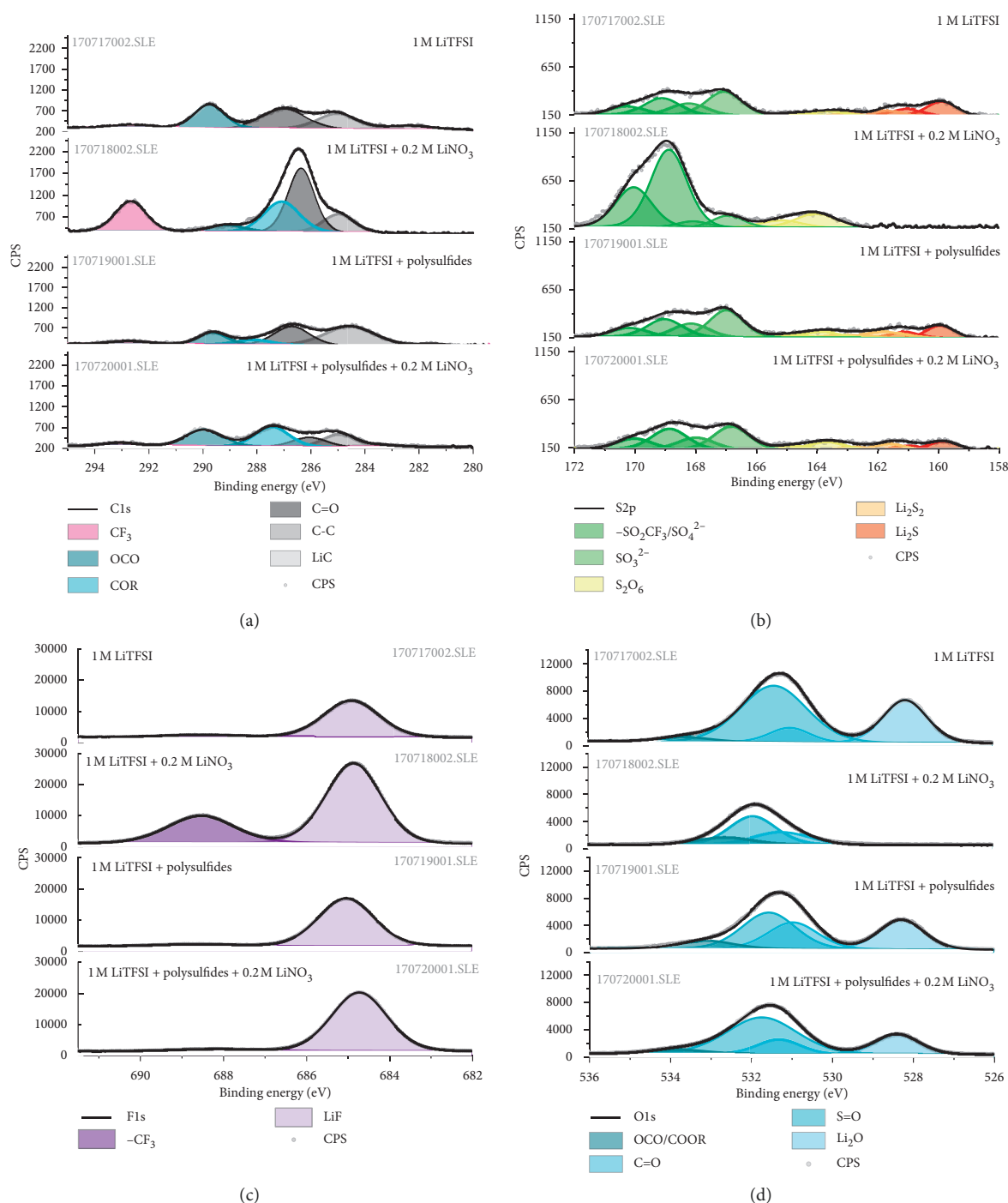
(a)

(b)

(c)

(d)

FIGURE 3: C1s (a), S2p (b), F1s (c), and O1s (d) core-level XPS spectra of the SEI layer of all four samples under investigation (see Table 1). The spectra are recorded after 30 min sputtering with Ar+. The individual components are presented in different colors. The envelope peaks are colored in black. The spectral intensity is presented as received (in counts per seconds, CPS) without further normalizations.

polysulfide-containing, and combined electrolytes, the SEI formed in the individually added $LiNO_3$ shows only the presence of highly oxidized +4, +5, and +6 sulfur states. This phenomenon can be explained by the overall increase in LiTFSI decomposition products, which is detected by the enhancement of CF_3 levels (see C1s core-level peaks). Therefore, it can be anticipated that $LiNO_3$ favors the

oxidation of any sulfur below maximum oxidation state; otherwise, the presence of Li_2S or Li_2S_2 would be detectable as previously discussed by Li et al. and others [6, 7].

The oxygen distribution, shown in Figure 5(c), supports our results on the redox states of carbon and sulfur in the SEI. When $LiNO_3$ is added to the electrolyte, Li_2O formation is completely suppressed, and the relative quantity of
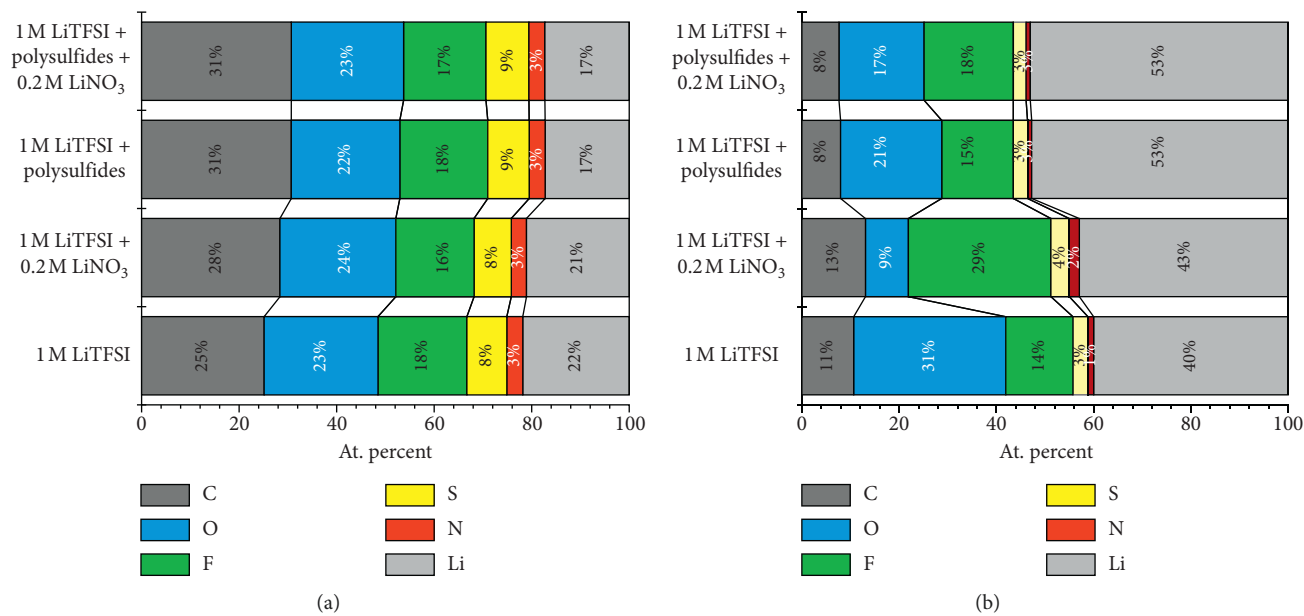
FIGURE 4: Calculated relative quantities of the elemental composition for spontaneously formed SEI layers in four different electrolytes: before (a) and after (b) 30 min sputtering with Ar$^+$.
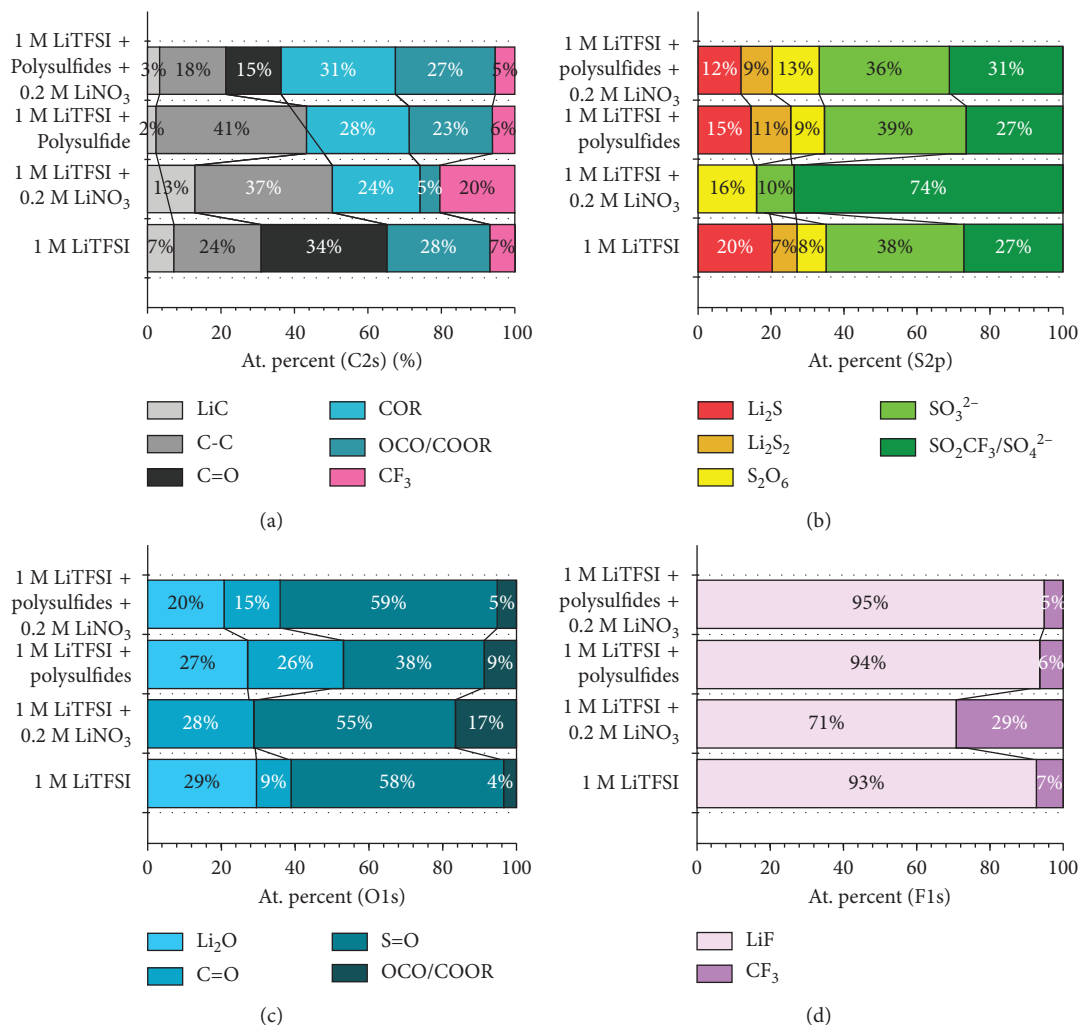

FIGURE 5: Relative distribution of carbon (a), sulfur (b), oxygen (c), and fluorine (d) containing chemical structures, detected after 30 min of sputtering with Ar$^+$ for the SEI layers formed by spontaneous passivation.

TABLE 1: Binding energy (BE) positions (eV) of the C-, S-, O-, and F-containing species from XPS spectra of a SEI layer formed after spontaneous passivation in DOL/TEGDME (7 : 3) and (i) 1 M Li[TFSI]; (ii) 1 M Li[TFSI] with LiNO$_3$; (iii) 1 M Li[TFSI] with polysulfides; and (iv) 1 M Li[TFSI] with polysulfides and LiNO$_3$, after sputtering (corresponding to Figure 3).

Chemical element	Chemical state	BE (eV)
C	Li-C	282.0
	C-C	285.0
	C=O	287.0
	COR	288.4
	O-C-O/COOR	290.0
	-CF$_3$	292.8
S	Li$_2$S	160.0
	Li$_2$S$_2$	161.8
	S$_x$O$_y$ ($2 \leq x \leq 8$, $0 \leq y \leq 6$)	162.5–164.5
	SO$_3{}^{2-}$	167.0
	$-SO_2CF_3/SO_4{}^{2-}$	169.0
O	Li$_2$O	528.3
	S=O	531.0
	C=O	531.6
	O-C-O/COOR	533.1
F	LiF	685.0
	CF$_3$	688.5

oxidized carbon species increases. On the other hand, the addition of PS to the electrolyte leads to an increase of the amount of C=O containing species, while concomitantly reducing the sulfur-oxygen proportion, possibly through reaction with already oxidized sulfur to form lower oxidized species. Besides, when both PS and LiNO$_3$ are added, the opposite tendencies of both additives negate each other, leading to the SEI that has a similar composition to the one formed in the reference electrolyte, however, with less Li$_2$O.

The results after deconvolution of the F1s core level (Figure 5(d)) show that the CF$_3$ signal in the SEI bulk is increased with respect to LiF, together with the total proportion of the fluorine signal (Figure 4(b)). This leads to the conclusion that LiF substitutes the inorganic parts (Li$_2$O and Li$_2$S/Li$_2$S$_2$) in the SEI formed by the assistance of LiNO$_3$, and this is probably one of the reasons for the exceptionally high R_{int} value. The high R_{int} of the SEI formed in the presence of PS can be explained as a combination of two factors: a low content of S=O bonds that facilitate Li$^+$ transport within the SEI [8] and a high relative amount of insulating C-C bonds. The fact that the R_{int} of the reference and combined electrolytes is comparable can also be clarified by their very similar oxidative state distribution, discussed previously.

3.2. Effect of Electrochemical Cycling. Electrochemical impedance spectroscopy in symmetric Li-Li electrode configuration has been performed after galvanostatic cycling of Li in full Li-S cells in presence and absence of LiNO$_3$. Before cycling, the cells were resting at OCP for 10 h in order to complete the growth of the spontaneously deposited SEI. The full cells were galvanostatically cycled, disassembled, and then pairs of Li metal anodes treated under identical conditions were reassembled in symmetric electrochemical cells for EIS measurement. Separate electrochemical cycling has been performed in symmetric Li-Li cells, in presence and

absence of additives. The results, plotted in Nyquist and Bode diagrams, are presented in Figures 6(a)–6(c). Comparing the impedance spectra of the cycled and self-passivated Li anodes, it becomes evident that the impedance after electrochemical cycling radically drops, $R_{int,c} << R_{int}$. This effect is even more pronounced for the SEI layers built in the presence of LiNO$_3$. Based on the latter observation, it can be expected that the formed SEI is not stable enough and probably deteriorates when cycled electrochemically. The onset of the phase minimum shifts markedly to higher frequencies when the Li anode is cycled with the LiNO$_3$-modified electrolyte (Figure 6(b)). This correlates well with the decrease in the total impedance (Figure 6(c)).

The morphology of the cycled Li surface in 1 M LiTFSI, DOL : DME and 1 M LiTFSI, DOL : TEGDME electrolytes changes evidently (Figures 7(a) and 7(b)). However, the initially present nano-objects (Li$_2$O and Li$_2$CO$_3$ particles, Figure S3) are still recognized on the Li surface. After electrochemical cycling, they look more anisodiametric for 1 M LiTFSI, DOL : DME and more isodiametric for the sample treated in 1 M LiTFSI, DOL : TEGDME. This indicates that SEIs spontaneously formed in these electrolytes are rather unstable during electrochemical cycling.

In contrast, the Li anodes cycled in the modified electrolytes appeared morphologically different. The Li sample, tested in the presence of LiNO$_3$, shows a deposition of nanosized (<50 nm) circular objects, closely resembling the morphology of the self-passivated Li in the same electrolyte for 10 h (Figure 7(c)). The observed morphological changes in this case are probably related to the instability of the initially formed SEI, followed by formation of more stable SEI when LiNO$_3$ is strongly depleted. After individual addition of PS, the Li surface seems to be covered with an inhomogeneous SEI layer, displaying a lower number of separate nano-objects (Figure 7(d)). In case of
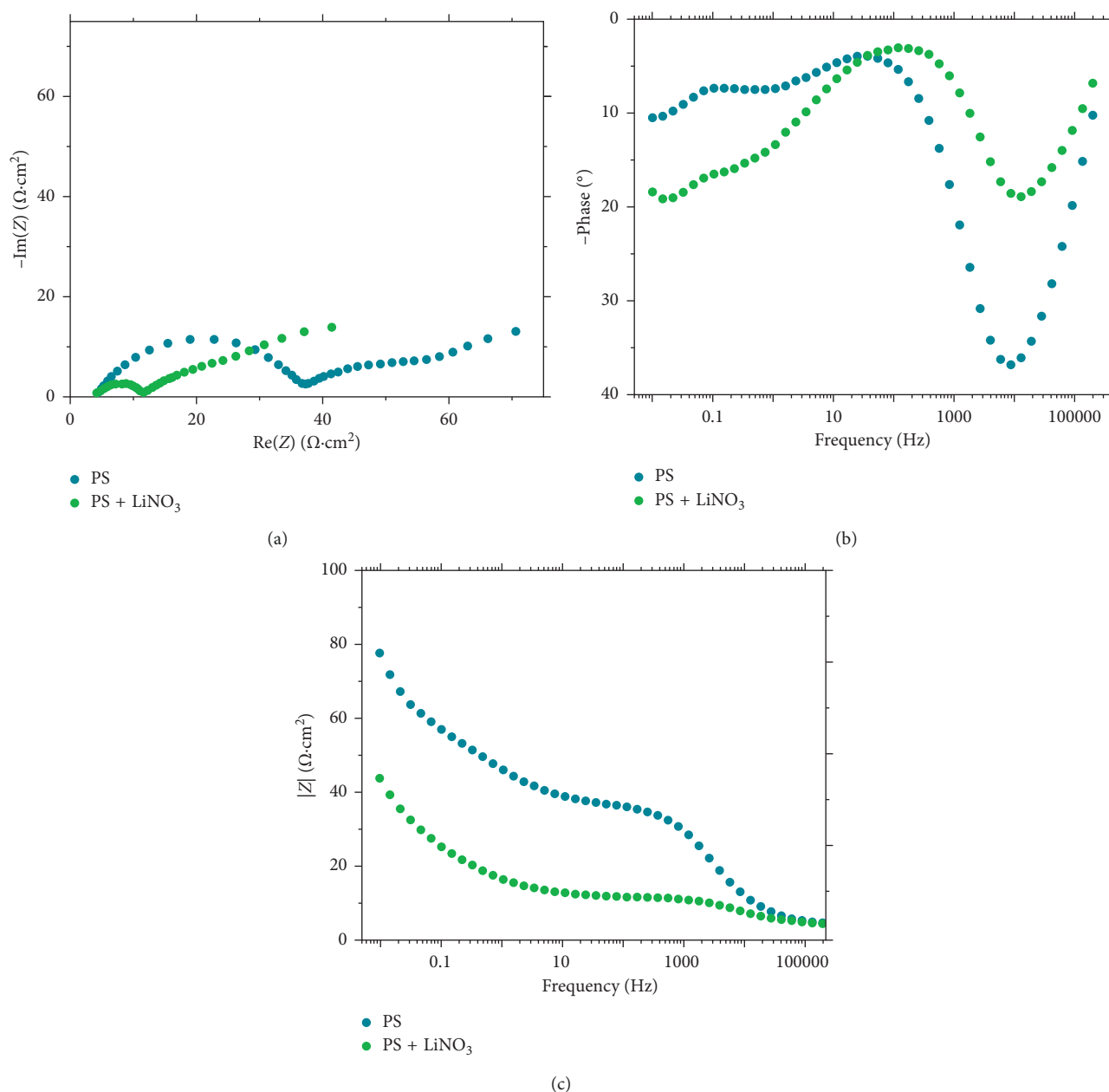
(a)

(b)

(c)

FIGURE 6: Nyquist and (a) Bode phase shift (b) and total impedance (c) diagrams for Li anodes tested in symmetric cells, after 25 constant current cycles at cycling rate C/5 with DOL/TEGDME (7 : 3) 1 M LiTFSI (blue) and additional 0.2 M LiNO$_3$ (green).

simultaneously modified electrolyte (PS + LiNO$_3$), the surface has a further enhanced morphological inhomogeneity, displaying big (>400 nm) aggregates and facilitating porous structure (Figure 7(e)).

Based on the visible morphological changes of the samples after electrochemical cycling in the presence of additives, it can be concluded that their surface is markedly modified, which indicates the reactivity of the added compounds and their additional interaction with the newly formed Li at any cycle. The rough and porous structure of the SEI formed in the combined (PS and LNO$_3$) electrolyte can probably facilitate the Li$^+$ mobility and finally decrease R_{int}.

Comparison of the elemental composition of the SEI layer before and after electrochemical cycling is presented in Figure 8. The XPS analysis was performed before (Figure 8(a)) and after 30 min Ar$^+$ sputtering (Figure 8(b)). The atomic distribution displays a much higher Li concentration on the surface and a decrease of the quantities for all other elements in the cycled sample (Figure 8(a)), which is probably the reason for the reduced R_{int} and total impedance Z. After sputtering, the SEI of the cycled cell (Figure 8(b)) shows a higher concentration of Li in exchange for lower F- and C-content, and the concentration of oxygen and sulfur remains unchanged. This chemical composition, however, is not a strong argument to explain the difference

135.0 nm

400.0 nm

1M LiTFSI, DOL : DME

(a)

200.0 nm

400.0 nm

1M LiTFSI, DOL : TEGDME

(b)

190.0 nm

400.0 nm

1M LiTFSI, DOL : TEGDME, LiNO₃

(c)

140.0 nm

400.0 nm

1M LiTFSI, DOL : TEGDME, PS

(d)

370.0 nm

400.0 nm
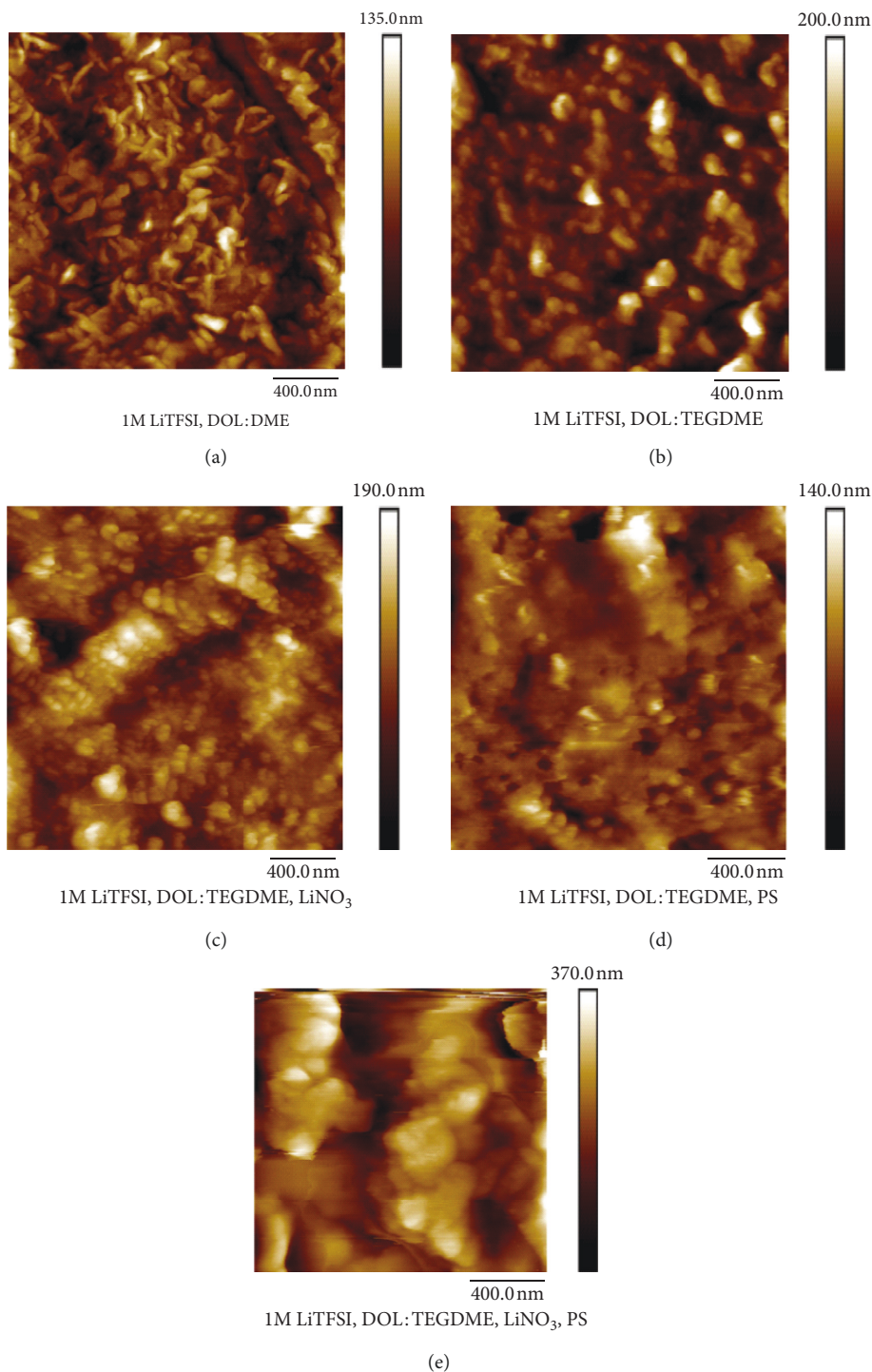
1M LiTFSI, DOL : TEGDME, LiNO₃, PS

(e)

FIGURE 7: Surface morphology of Li plates after symmetric Li-Li electrochemical cycling in 1 M LiTFSI, DOL : DME (7 : 3 vol.) (a), 1 M LiTFSI, DOL : TEGDME (b), 1 M LiTFSI, DOL : TEGDME, LiNO₃ (c), 1 M LiTFSI, DOL : TEGDME, PS (d), and 1 M LiTFSI, DOL : TEGDME, LiNO₃, PS (e).

in resistance by more than a factor of 10 between the self-passivated and cycled samples. Related to this, Li et al. have demonstrated that the morphology of the SEI on Li metal anodes can also play an important role in the ionic conductivity. The conclusion here would be that SEIs formed in resting cells (self-passivated Li) are more compact and therefore pose higher resistance for Li ions.

Figure 9 presents the relative concentration of carbon- and sulfur-containing species in the SEI formed after electrochemical cycling in cells with 1 M LiTFSI, DOL : TEGDME and PS electrolyte. It can be observed that CF_3 fragments (decomposition product of TFSI) can be detected only on the SEI surface. High relative concentration of Li_2S_2 can be distinguished before sputtering, apparently resulting
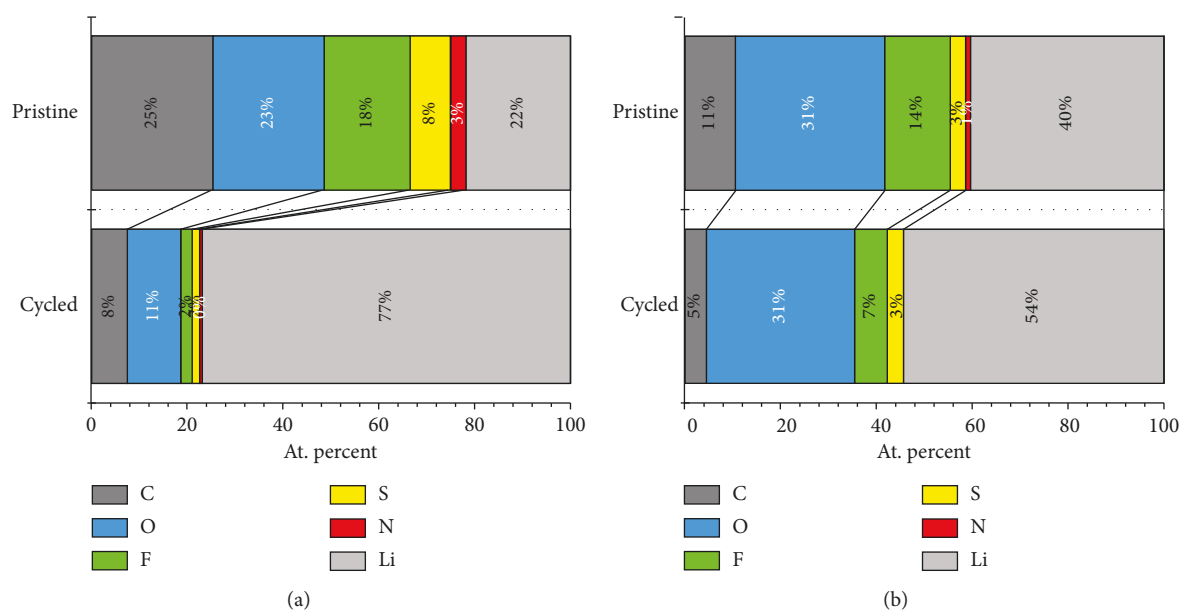
FIGURE 8: Calculated relative quantities of the elemental composition for the SEI layers after self-passivation and electrochemical cycling in a full Li-S cell with 1M LiTFSI, DOL : TEGDME electrolyte, before (a) and after (b) 30 min Ar sputtering time.
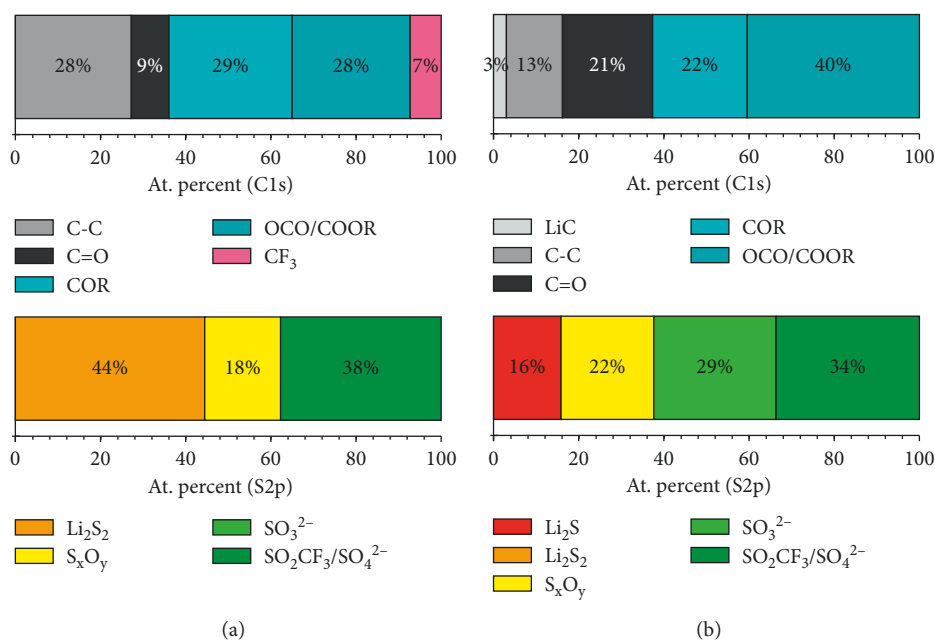

FIGURE 9: Relative distribution of carbon (a) and sulfur (b) containing chemical structures detected before (left) and after (right) 30 min of Ar sputtering for the SEI layers after electrochemical cycling in 1 M LiTFSI, DOL : TEGDME and PS electrolyte.

from the strong polysulfide adsorption. After electrochemical cycling, Li_2S_2 is no longer evident and only Li_2S remains distributed in the SEI volume.

4. Conclusions

This work combined electrochemical impedance spectroscopy, photoelectron spectroscopy, and atomic force microscopy to form a complete systematic picture on the influence of polysulfides and lithium nitrate on the SEI

formation in assembled and cycled electrochemical cells with TEGDME-based electrolyte. The impedance of the symmetric cells spontaneously increased after individual addition of polysulfides and $LiNO_3$ and decreased when a combination of both additives was simultaneously applied. Polysulfides were found to reduce the overall oxidation state of sulfur and carbon within the SEI, while lithium nitrate was found to increase it. The SEI layers spontaneously formed in the nonmodified electrolytes have initially a nanoscale morphology and exhibit a

tendency for smoothing with time, indicating their compactness. In the presence of polysulfides and mixture of polysulfides + LiNO$_3$, the SEIs develop a rough, inhomogeneous structure. The individual addition of LiNO$_3$ leads to instability of the passivation layer. The electrochemical cycling influenced visibly the SEI morphology. While the pristine Li topology can be still identified after electrochemical cycling in the non-modified electrolytes, the samples treated in the presence of PS displayed irregular porous morphology. The redistribution of the SEI composition and the rough/porous structure (typical for the combined electrolyte) is advantageous regarding the electrochemical performance and stability.

Data Availability

The data used to support the findings of this study are available from the corresponding author upon request.

Conflicts of Interest

The authors declare that there are no conflicts of interest regarding the publication of this paper.

Acknowledgments

Supplementary Materials

Detailed electrochemical impedance measurements (Nyquist and Bode plots) are given in Figures S1 and S2, and AFM imaging is shown in Figures S3–S6. (*Supplementary Materials*)

References

[1] P. Bai, J. Li, F. R. Brushetta, and M. Z. Bazant, "Transition of lithium growth mechanisms in liquid electrolytes," *Energy & Environmental Science*, vol. 9, no. 10, pp. 3221–3229, 2016.

[2] J. Zheng, M. H. Engelhard, D. Mei et al., "Electrolyte additive enabled fast charging and stable cycling lithium metal batteries," *Nature Energy*, vol. 2, no. 3, p. 17012, 2017.

[3] M. N. Obrovac and V. L. Chevrier, "Alloy negative electrodes for Li-ion batteries," *Chemical Reviews*, vol. 114, no. 23, pp. 11444–11502, 2014.

[4] M. Gauthier, T. J. Carney, A. Grimaud et al., "Electrode–electrolyte interface in Li-ion batteries: current understanding and new insights," *Journal of Physical Chemistry Letters*, vol. 6, no. 22, pp. 4653–4672, 2015.

[5] Q. Chen, K. Geng, and K. Sieradzki, "Prospects for dendrite-free cycling of Li metal batteries," *Journal of the Electrochemical Society*, vol. 162, no. 10, pp. A2004–A2007, 2015.

[6] A. Manthiram, Y. Fu, S.-H. Chung, C. Zu, and Y.-S. Su, "Rechargeable lithium–sulfur batteries," *Chemical Reviews*, vol. 114, no. 23, pp. 11751–11787, 2014.

[7] W. Li, H. Yao, K. Yan et al., "The synergetic effect of lithium polysulfide and lithium nitrate to prevent lithium dendrite growth," *Nature Communications*, vol. 6, no. 1, p. 7436, 2015.

[8] D. Aurbach, E. Pollak, R. Elazari, G. Salitra, C. S. Kelley, and J. Affinito, "On the surface chemical aspects of very high energy density, rechargeable Li–sulfur batteries," *Journal of the Electrochemical Society*, vol. 156, no. 8, pp. A694–A702, 2009.

[9] S. Ferrari, E. Quartarone, P. Mustarelli et al., "A binary ionic liquid system composed of N-methoxyethyl-N-methylpyrrolidinium bis(trifluoromethanesulfonyl)-imide and lithium bis(trifluoromethanesulfonyl)imide: a new promising electrolyte for lithium batteries," *Journal of Power Sources*, vol. 194, no. 1, pp. 45–50, 2009.

[10] M. Dahbi, D. Violleau, F. Ghamouss et al., "Interfacial properties of LiTFSI and LiPF$_6$-based electrolytes in binary and ternary mixtures of alkylcarbonates on graphite electrodes and celgard separator," *Industrial & Engineering Chemistry Research*, vol. 51, no. 14, pp. 5240–5245, 2012.

[11] A. Martinelli, A. Matic, P. Jacobsson, L. Börjesson, A. Fernicola, and B. Scrosati Phase, "Behavior and ionic conductivity in lithium bis(trifluoromethanesulfonyl)imide-doped ionic liquids of the pyrrolidinium cation and bis(trifluoromethanesulfonyl)imide anion," *Journal of Physical Chemistry B*, vol. 113, no. 32, pp. 11247–11251, 2009.

[12] P. M. Bayley, G. H. Lane, N. M. Rocher et al., "Transport properties of ionic liquid electrolytes with organic diluents," *Physical Chemistry Chemical Physics (PCCP)*, vol. 11, no. 33, pp. 7202–7208, 2009.

[13] M. Agostini, S. Xiong, A. Matic, and J. Hassoun, "Polysulfide-containing glyme-based electrolytes for lithium sulfur battery," *Chemistry of Materials*, vol. 27, no. 13, pp. 4604–4611, 2015.

[14] J. Conder, C. Villevieille, S. Trabesingera, P. Novák, L. Gubler, and R. Bouchet, "Electrochemical impedance spectroscopy of a Li–S battery: part 1. Influence of the electrode and electrolyte compositions on the impedance of symmetric cells, Electrochim," *Electrochimica Acta*, vol. 244, pp. 61–68, 2017.

[15] S. Xiong, K. Xie, Y. Diao, and X. Hong, "Properties of surface film on lithium anode with LiNO$_3$ as lithium salt in electrolyte solution for lithium–sulfur batteries," *Electrochimica Acta*, vol. 83, pp. 78–86, 2012.

[16] S. Xiong, Y. Diao, X. Hong, Y. Chen, and K. Xie, "Characterization of solid electrolyte interphase on lithium electrodes cycled in ether-based electrolytes for lithium batteries," *Journal of Electroanalytical Chemistry*, vol. 719, pp. 122–126, 2014.

[17] D.-R. Chang, S.-H. Lee, S.-W. Kim, and H.-T. Kim, "Binary electrolyte based on tetra(ethylene glycol) dimethyl ether and 1,3-dioxolane for lithium–sulfur battery," *Journal of Power Sources*, vol. 112, no. 2, pp. 452–460, 2002.

[18] B. Vincent Crist, "A review of XPS data-banks," in *XPS Reports*, vol. 1, pp. 1–52, XPS International, 2007.

[19] D. A. Shirley, "High-resolution X-ray photoemission spectrum of the valence bands of gold," *Physical Review B*, vol. 5, no. 12, pp. 4709–4714, 1972.

[20] J. H. Scofield, "Hartree-slater subschell photoionization cross-sections at 1254 and 1487 eV," *Journal of Electron Spectroscopy and Related Phenomena*, vol. 8, no. 2, pp. 129–137, 1976.

[21] M. Steinhauer, M. Stich, M. Kurniawan et al., "In situ studies of solid electrolyte interphase (SEI) formation on crystalline carbon surfaces by neutron reflectometry and atomic force microscopy," *ACS Applied Materials & Interfaces*, vol. 9, no. 41, pp. 35794–35801, 2017.